Proceedings of FEDSM2005:
2005 ASME Fluids Engineering Division Summer Meeting and Exhibition
June 19-23, 2005, Houston, TX, USA

DRAFT **FEDSM2005-77354**

COMPUTATIONAL STUDY OF PRESSURE PULSATION IN A MEDIUM SPECIFIC SPEED PUMP

Serguei Timouchev
InteRe Ltd
E-mail: irico@online.ru

Andrey Aksenov
Tesis Ltd

ABSTRACT

The centrifugal pump of high specific speed with a diagonal type of impeller flow is studied experimentally and numerically. 2D and 3D numerical methods are used with applying acoustics – vortex equations.

Increasing energetic parameters of centrifugal pumps requires a more complex geometry of the impeller and volute as one need to raise the specific speed of the pump to provide a higher efficiency value. The pump of higher specific speed has an impeller with curved blades and diagonal meridional section. The flow outgoing the impeller has an essential axial component of velocity. Thus the two dimensional approach will not give the accurate prediction of pressure pulsations in the volute casing. This is why the new 3-dimensional method has been elaborated for this task. The 3D computational results of pressure pulsation are compared with those obtained by 2D-computation Measurements show that in the beginning of volute, in the pseudo-sound zone, amplitude of Blade Passing Frequency (BPF) spectral component is higher than that at the pump outlet by an order of magnitude. 3-Dimensional analysis gives a good agreement with experimental data while 2D prediction underestimates the BPF amplitude in the beginning of volute.

INTRODUCTION

Blade-passing frequency (BPF) pressure pulsation and tone noise and vibration are generated by a step-wise non-uniformity of flow parameters at the centrifugal impeller exit that causes vortex perturbations. These perturbations result from the motion of periodically inhomogeneous flow with a peripheral velocity U_2 of the impeller relatively to the pump casing. Convective transposition of vortex perturbations is considered as the main physical reason of non-stationary generation process of BPF pressure pulsations in the pump. It is well known that the pressure pulsation field in the working cavity of centrifugal pumps or ventilators may be represented as a combination of pseudo-sound oscillations ("vortex mode") and acoustic waves ("acoustic mode"). The vortex perturbations are exponentially damped within a zone of 20% of impeller tip radius. They generate acoustic oscillations propagating in the pump's working cavity and the outlet pipe at the speed of sound.

For the solution of this problem a method that is based on splitting the equations of compressible fluid dynamics into two modes, vortex and acoustic, is proposed[i]. In this case, the non-linear equations for the unsteady vortex motion of an incompressible liquid are solved with a bigger time step. Wave equation in respect to the pressure pulsation, which takes into account acoustic impedances on the boundaries of computational domain, is solved by a highly effective explicit method. As a result, the whole processor time reduces and accuracy of prediction of pressure pulsation improves.

The current trend of increasing energetic parameters of centrifugal pumps requires a more complex geometry of the impeller and volute as one need to raise the specific speed of the pump to provide a higher efficiency value. The pump of high -- medium specific speed has an impeller with curved blades and diagonal meridional section. The flow outgoing the impeller has an essential axial component of velocity. Thus the two dimensional approach will not give the accurate prediction of pressure pulsations in the volute casing. This is why the new 3-dimensional method has been elaborated for this task. The 3D computational results of pressure pulsation are compared with those obtained by 2D-computation. The unsteady hydrodynamic interaction of the rotor-outlet flow with the fixed vane cascade or volute tongue of a pump casing is the basic source of noise and vibration. Because of such an interaction acoustical disturbances are formed. They extend upstream and downstream with the speed of sound, reflect from the input and output impedances. Near the rotor, in the source of noise oscillations, is a region of pseudo-sound perturbations; they extend with the speed of flow and rapidly attenuate downstream.

Thus inside the pump there are two modes even two zones of perturbations, which differ in the physical nature of oscillations and equations describing their behavior. The first

mode is pseudo-sound oscillations caused by unsteady vortex motion of liquid as an incompressible fluid. The second mode is the acoustic oscillations, which extend throughout entire zone of flow with the speed of sound.

It is known that application of common CFD codes for compressible fluid proves to be ineffective for the solution of problem of optimization of design regarding pressure pulsation, especially for the acoustical part of pressure field. Some works were published[ii], in which the methods of prediction of pressure pulsation were developed by a direct computation of non-stationary two-dimensional flow in a centrifugal impeller and volute with solution of averaged Navier-Stokes equations and k-ε model of turbulence. Other approaches[iii],[iv] used solutions of hydrodynamic equations accompanied with laser anemometric measurements. The most promising approaches[v],[vi] proposes 2 – 3 steps computational procedure including solution of Navier-Stokes equation with Large Eddy Simulation (LES) method and consecutive application of an appropriate integral method for resolving far-field noise.

GOVERNING EQUATIONS

For the solution of this problem the method is proposed[vii], which is based on splitting the equations of compressible fluid dynamics into two modes - vortex and acoustic. In this case non-linear equations for unsteady vortex motion of an incompressible liquid are solved with a bigger time step. Wave equation relative to the pressure pulsation taking into account acoustic impedances on the borders of computational domain is solved by an explicit method. As a result a whole processor time for both modes of oscillations has reduced and accuracy of prediction for the acoustical mode is increased. The method is included into 2-D and 3-D software packages.

For prediction pressure pulsation and noise in the outlet pump section, the mathematical model is based on a representation of the fluctuating flow velocity field V as a combination of vortex and acoustic modes,

$$\mathbf{V} = \mathbf{U} + \nabla\varphi = \mathbf{U} + \mathbf{V_a} \qquad (1)$$

Where $\mathbf{U}$ - Velocity of transitional and rotational motion of an incompressible fluid (vortex mode)

$\mathbf{V_a}$ - Velocity of pure deformation (the acoustic mode)

φ - Acoustic potential

This gives the acoustic-vortex wave equation in terms of enthalpy oscillation i in the isentropic flow of a compressible fluid (a – mean sound velocity):

$$\frac{1}{a^2}\frac{\partial^2 i}{\partial t^2} - \Delta i = \nabla(\nabla(\tfrac{1}{2}U^2) - \mathbf{U}\times(\nabla\times\mathbf{U})) \qquad (2)$$

Right hand side of this equation represents the source function, defined from the velocity field of vortex mode flow. It is determined from the solution of unsteady equations of incompressible fluid with appropriate boundary conditions. It must be noted that it differs in its source term from from the well-known Lightill[viii] equation. There is a simplification with regard to convection of acoustical perturbations by the fluid flow. For higher frequencies it will be more accurate to use the operator $\partial/\partial t + \mathbf{U}\cdot\nabla$ of substantial derivative instead of $\partial/\partial t$, where U is the vector of the vortex mode velocity.

Right hand side of this equation represents the source function, defined from the velocity field of vortex mode flow. It is determined from the solution of unsteady equations of incompressible fluid.

Mathematical model of incompressible liquid flow bases on Navier-Stokes equation

$$\frac{\partial\mathbf{U}}{\partial t} + \nabla(\mathbf{U}\otimes\mathbf{U}) = -\frac{\nabla P}{\rho} + \frac{1}{\rho}\nabla((\mu+\mu_t)(\nabla\mathbf{U} + (\nabla\mathbf{U})^T) \qquad (3)$$

with taking into account the continuity equation for incompressible liquid $\nabla\cdot\mathbf{U} = 0$;

The well-known $k-\varepsilon$ model of turbulence is used to determine the turbulent viscosity by relation

$$\mu_t = 0.09\cdot\rho\cdot\frac{k^2}{\varepsilon} \qquad (4)$$

Initial values of kinetic energy and dissipation were calculated automatically during the first step of computation.

Navier-Stokes equations are solved by splitting method with the implicit algorithm and high-order numerical scheme for convective transfer terms. The advantage of the method is that it is possible to reduce processing time by making computation on a rough grid, refining the grid when approaching to the convergent oscillatory solution. Iterative procedure of the vortex mode equations goes up to a convergent periodical solution and subsequent definition of the source function of the equation (2). Initial condition of the vortex mode flow is zero pressure and velocity in the entire computational domain. Boundary condition on the wall is represented by a numerical equivalent of the well known logarithmic law for the tangential component U of the velocity vector.

It can be found by the following expression

$$\frac{U}{U_*} = \begin{cases} y^+, & y^+ < y_*^+ \\ u^+ & y^+ \ge y_*^+ \end{cases} \qquad (5)$$

where $U_* = \sqrt{\frac{\tau_w}{\rho}}$ is the friction velocity, τ_w – wall shear stress and TBL kinematic parameters defined by the following formulas

$$u^+ = \frac{1}{\kappa}\ln(Ey^+)$$

$$y^+ = \frac{\rho U_* h}{\mu} \qquad (6)$$

where $\kappa = 0.41$, $E = 9$ and $y_*^+ \approx 11$.

The solution of the acoustic-vortex equation is divided into two steps - computation of the incompressible flow for the determination of the source function and solution of the inhomogeneous wave equation for the determination of pressure pulsation that can be represented like a sum of acoustic and vortex oscillation.

The problem of pressure oscillation field determination splits into two or three main steps. The first one is the incompressible liquid flow analysis in the impeller (rotor) to obtain unsteady boundary condition of the vortex mode flow.

This boundary condition can be represented in the form of a distribution of rotating parameters' "attached " to the impeller exit diameter. The second step is the unsteady vortex mode flow computation into the working cavity of a pump with consequential determination of the source function, and the third one is solution of the wave equation in respect of pressure oscillations. By using a local complex specific acoustic impedance Z, the boundary condition for the acoustic mode can be put in the form

$$\frac{\partial (i_k - I_k)}{\partial n} = -\frac{k}{a Z_k} \frac{\partial (i_k - I_k)}{\partial t} \qquad (7)$$

where k is a number of BPF harmonic, n – normal direction to the boundary, I – enthalpy oscillation in the incompressible flow.

In 2D analysis the vortex mode flow is computed in 2 steps. In the first step the flow around rotor is defined by the discrete vortex method that applies "sliding-break-point" conditions on blades. In the second step the unsteady Euler equations are solved for the turbulent flow in the volute casing. Then the source function of the wave equation is defined from the unsteady velocity field of the vortex mode.

The 3D numerical procedure is based on non-staggered Cartesian grid with adaptive local refinement and a sub-grid geometry resolution method for description of curvilinear complex boundaries. For vortex mode flow, unsteady Navier-Stokes equations are solved with applying standard k-ε turbulence model. Our experience shows that for modeling of steady oscillatory BPF phenomena such an approach brings successful results. Using Direct Numerical Simulation (DNS) is also possible by applying a simple non-slipping boundary condition on the wall. The numerical procedure provides stability of the solution even on a relatively rough grid. Certainly the accuracy of such a modeling must be validated in each case. Iterative procedure goes up to convergence to a periodical solution and subsequent definition of the source function.

Initial condition is zero pressure and velocity in entire computational domain. On rigid walls the logarithmic velocity profile is applied as a boundary condition for the turbulent flow. At the outer boundary free-outlet flow condition is used with linear extrapolation of velocity from inner nodes.

Finally wave equation is solved relatively to pressure oscillation using an explicit numerical procedure. Zero pulsatory pressure is an initial condition for solution of the wave equation. The local complex specific acoustic impedance is used to define boundary conditions for the acoustical part of the pressure field.

TESTING ON THE AIR PUMP MODEL

The computational method has been tested on the air pump model[ix]

The air pump represents a simple model of centrifugal pump with 2-dimensional volute and conic diffuser with the open outlet section. It has been experimentally studied including measurements of pressure pulsation in more than 300 points.

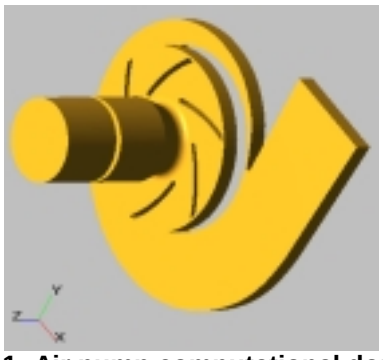

Fig. 1: Air pump computational domain

In Fig. 1 one can see the typical computational domain i.e. the "liquid volumes" representing inlet pipe, impeller and volute casing. They are arranged in the mathematical space to be computed on one grid and linked by "sliding surface" interfaces. Sliding surfaces is actually an interface for transfer the data from rotating to the motionless part of the physical domain and vice-versa

The important issue in the adequate prediction of pressure pulsation is accurate modeling of flow parameters at the impeller outlet. An example of unsteady 3D computation is presented in Fig. 1.

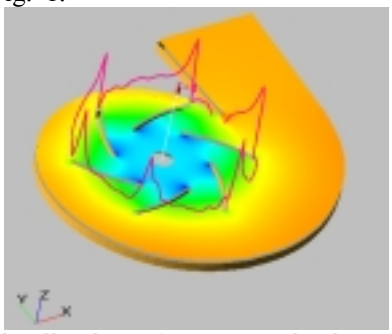

Fig. 2: Distribution of pressure in the volute and impeller outlet radial velocity

Resulting distribution of the radial; and circumferential components of absolute velocity at the impeller outlet circle is presented in Fig. 2. It agrees with previous 2D computations and other experimental data. The maximal radial velocity locates near pressure side and this point corresponds to the minimum of the circumferential velocity.

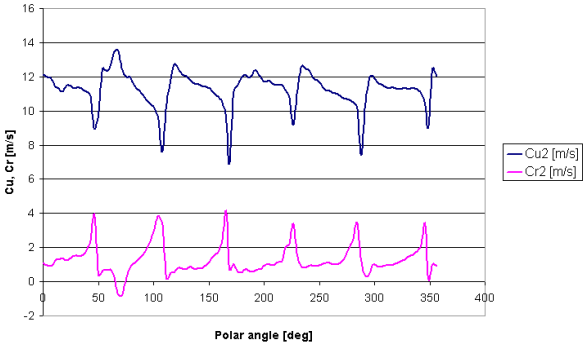

Fig. 3: Radial and circumferential component at the impeller outlet

Computed pressure pulsations are compared at the inlet of the pump and at the beginning and throat of the volute (Fig. 4) for the rotation speed 1500 RPM and flow rate 13.6 l/s.

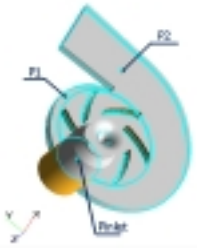

Fig. 4: Location of points

At the pump inlet (Fig. 5) the amplitude of pressure pulsation is minimal, the first BPF harmonic is about 0.6 Pa. The maximum pressure pulsation level takes place in the beginning of volute with the amplitude of the the first BPF tone more than 3 Pa (Fig. 6) whilst in the volute throat the BPF amplitude is less than 2 Pa (Fig. 7). It is well agrees with experimental data[ix] and previous 2D computations[i].

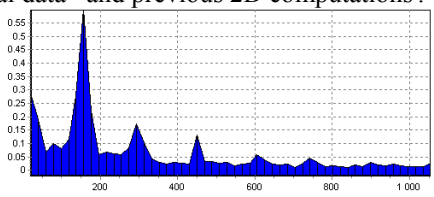

Fig. 5: Amplitude spectrum (Pa) at the inlet

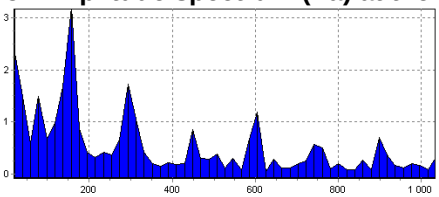

Fig. 6: Amplitude spectrum (Pa) at the P1

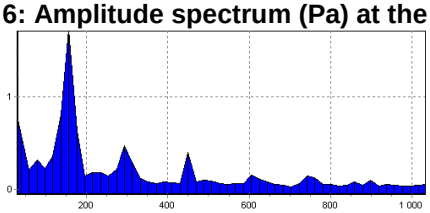

Fig. 7: Amplitude spectrum (Pa) at the P2

3D GEOMETRY INPUT

The method is applied for computational study of the diagonal pump of medium specific speed.

To build the computational grid a 3D Geometry surface must be specified by a set of elementary surfaces (facets). This kind of representation is used by different CAD systems and can be supplied in the form of CAD data specific format like VRML etc.

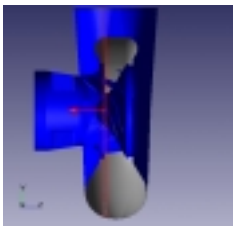

Fig. 8: 3D geometry – side view

The assembly geometry of the diagonal pump is shown in Fig. 8 and Fig. 9.

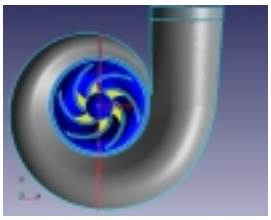

Fig. 9: SD geometry – plane view

By red color line on these figures are shown main sections (plane and meridional) for representation of computational results.

COMPUTATIONAL GRID

The numerical procedure is based on non-staggered Cartesian grid with adaptive local refinement and accurate resolution of curvilinear boundaries, like blade surface, by using polyhedron cells. The initial "parent" rectangular cell intersected by a curvilinear surface is disjoined onto new polyhedron cells formed by the facets of blade surface and the original cell faces. The grid of the first level is an ordinary structured grid. Each cell of the grid can be subdivided (when adaptation occurs) by eight cells of a higher-level grid and these cells can be subdivided in the next level of adaptation. The adaptive locally refined rectangular grid is obtained by the adaptation of 2 levels. This gave a reasonable value of processing time – a few hours for each impeller turn and the accuracy level.

In Fig. 10 and Fig. 11 below one can see an example of computational grid of the second level of adaptation, when the initial grid of about 6000 calculated cells is adapted near wall boundaries by splitting the initial parent cells on a smaller cells by two times. This procedure is applied for all stator and rotor walls and for sliding surfaces where there is an interface between rotating and motionless volumes.

Computations for definition of head characteristics are completed on the computational grid of the first level of adaptation. Detailed studies of pressure pulsation spectra are made on the grid of the second level.

In the Fig. 11 one can see that in the computational domain the physical liquid volume is divided on to three regions, namely "Inlet", "Rotor" and "Stator". Mathematically these regions are connected to each other with "sliding surfaces".

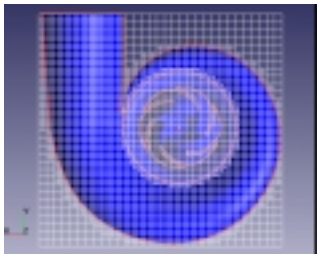

Fig. 10: Computational grid of the second adaptation level; Plane view

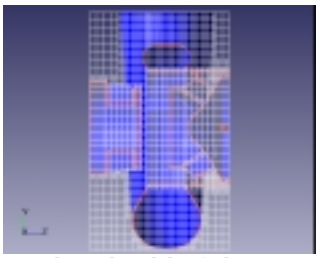

Fig. 11: Computational grid of the second adaptation level; Side view

OPERATION MODES OF THE MEDIUM SPECIFIC SPEED WATER PUMP

There are studied three main operation modes of the pump at the constant rotation speed 1485 rpm. These free modes correspond:

Qmin = 33 % of BEP flow rate
Qnom = 100 % of BEP flow rate
Qmax = 120 % of BEP flow rate

INFLUENCE OF THE IMPELLER DIAMETER

In the previous section it was shown that the impeller 413 brings the rise of head in all flow rates in a full accordance with experimental head characteristic.

It is found the unsteady static pressure maps and velocity vectors do not differ qualitatively except the overall level of the static pressure and a more non-uniformity of pressure field near the tongue for the impeller 413.

It is logical to assume that with impeller 413 the flow disturbances around the volute tongue are more strong because of reduction of the radial gap (D3-D2)/D2.

On the non-optimal modes of operation the difference increases due to secondary flow phenomena.

Under the maximal flow rate, with impeller 413, the small zone of separation becomes more distinct on the suction side of the volute tongue. Velocity vectors in meridional plane for maximal flow rates are similar for both impeller designs.

Regarding the minimal flow rate it can be noted an essential change in the velocity vector field shown in Fig. 12, that is with impeller 413 the energy of back –flow before the inlet ribs reduces, but the swirl near impeller inlet edges intensifies.

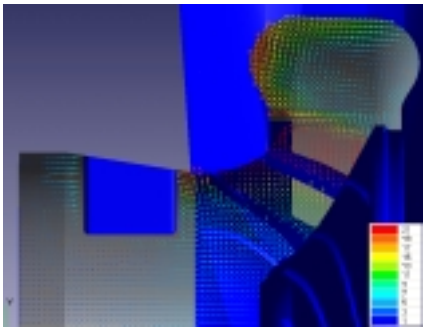

Fig. 12: Velocity vectors at the minimal flow rate; impeller 413

UNSTEADY INLET FLOW

Two inlet planes were chosen to illustrate the particularities of unsteady flow under minimal flow rate with impeller 380. One plane is before the ribs (upstream) and the second is after the ribs, near inlet edges of the impeller.

Under the nominal flow rate there is no back - flow in the inlet section. There local minimums of velocity against the inlet ribs.

There is a considerable recirculation with 50% of back-flow under minimal flow rate (Fig. 13) that reflects on static pressure distribution (Fig. 14).

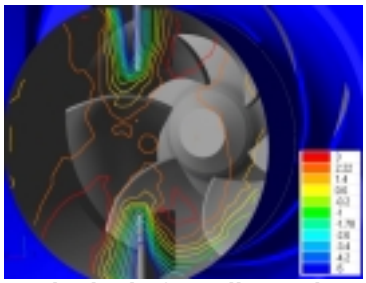

Fig. 13: Inlet velocity before ribs at the minimal flow rate; Impeller 380 mm

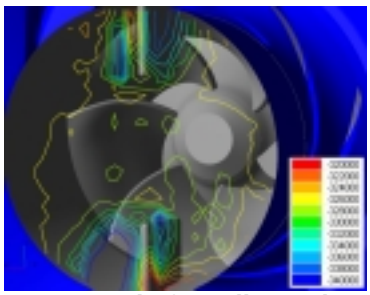

Fig. 14: Inlet pressure before ribs at the minimal flow rate; Impeller 380 mm

The more interesting result one can get from the velocity and pressure distribution in the plane after the ribs (see Fig. 15 and Fig. 16).

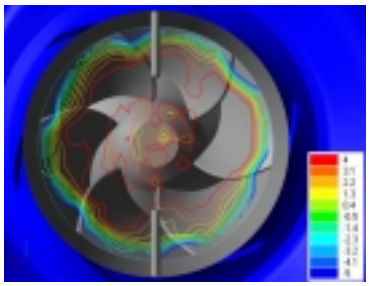

Fig. 15: Inlet velocity after ribs (closer to the impeller) at the minimal flow rate; Impeller 380 mm

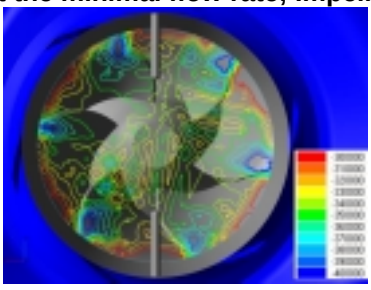

Fig. 16: Inlet pressure after ribs (closer to the impeller) at the minimal flow rate; Impeller 380 mm

Here velocity and pressure have a periodical structure connected with blades. Thus under minimal flow rate inlet flow can be an additional source of BPF type. Recirculation flow from the impeller (connected with rotating blades) can interact with inlet ribs in the same manner as the impeller outflow interacts with a bladed stator or the volute tongue.

PRESSURE PULSATION

The most important feature of this pump regarding pressure pulsation is the relatively higher level of the BPF amplitude at the beginning of volute (P1).

DISTRIBUTION OF AMPLITUDE ALONG THE VOLUTE LENGTH

Pressure pulsation measurements have been completed in points P1, P3, and P4 and in the outlet pipe $(P5)^x$.

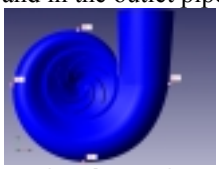

Fig. 17: Location of points of pressure pulsation study-Impeller 380

According to the measurements, the characteristic features of the pump are strong oscillations near the volute tongue (point P1); five times smaller amplitudes at the outlet (points P4, P5) and minimal pressure pulsation at the volute bottom (point P3). It must be noted the last result is obviously connected with some particularities of the measurement point although in computation the lower level of pressure pulsation in this zone of volute is also detected.

Using 2D computation it is impossible to model such a distribution of the BPF amplitude along the volute length. If one makes a 2D computation simulation to get a hypothetic qualitative result as shown Fig. 18 and Fig. 19 and comparable to above experimental values, then he must assumes that it corresponds to the "open-end" impedance condition (i.e. zero impedance) at the pump outlet and a larger impeller diameter with 11% radial gap (between impeller tip radius and volute tongue) whereas in the actual pump there is a 25% radial gap.

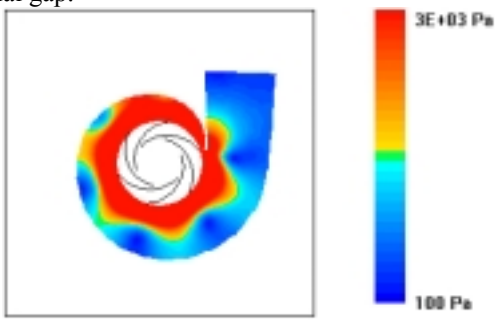

Fig. 18: 2D computation; 1st BPF amplitude; Open-end impedance

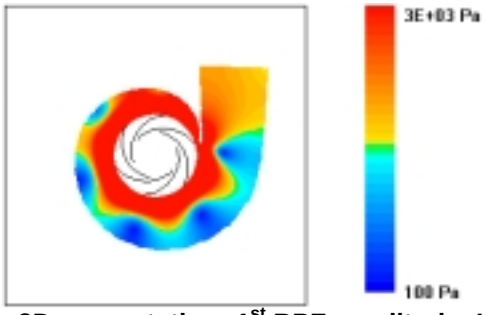

Fig. 19: 2D computation; 1st BPF amplitude; Infinite-pipe impedance

With the normal "infinite-pipe" impedance condition (i.e. unit specific impedance) (see Fig. 19) the 2D simulation gives more than 1000 Pa of BPF amplitude at the pump outlet. The effect of radial gap is presented in Fig. 20 (for P5).

It must be noted that Harmony code (2D model) is validated and applicable to centrifugal pumps with specific speed n_s<150 ($n_s = 193.3\omega\sqrt{Q}H^{-3/4}$, SI units rad/s, m^3/s, J/kg are applied). For the pump studied n_s value is about 300. Thus, the 2D method cannot treat accurately 3D behavior of pseudo-sound pulsation in the volute of this diagonal pump.

As it was shown before, the unsteady velocity field in the volute has an essential 3D structure that generates a secondary spiral flow. This effect increases hydrodynamic interaction between the flow outgoing from the impeller and the volute tongue, resulting in a higher level of pressure pulsation at the beginning of the volute.

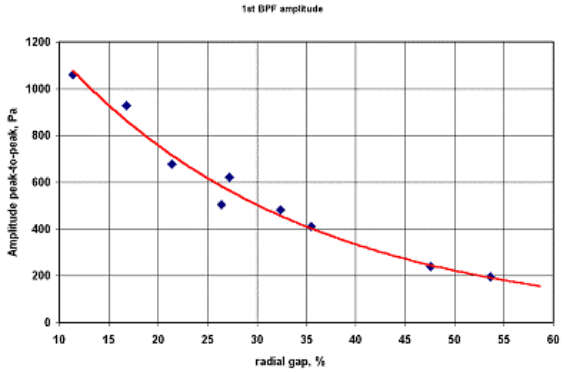

Fig. 20: 2D estimation of the influence of the radial gap on the outlet BPF amplitude

Comparing measured amplitude with 2D computational results in Fig. 21 one can conclude that 2D prediction is still valid for the outlet section of the pump.

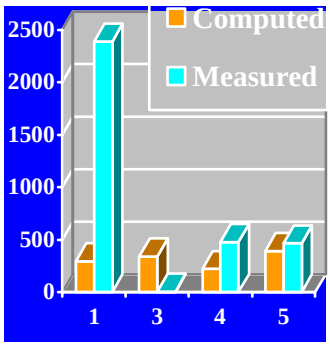

Fig. 21: Comparison of measurement with 2D computation

3D computation for the BEP flow rate is completed on the grid of the second level of adaptation. It brings at point P1 the signal and spectrum shown in Fig. 22; BPF component dominates in the spectrum in agreement with experimental result but the RMS value of amplitude is smaller by 19% than the measured level.

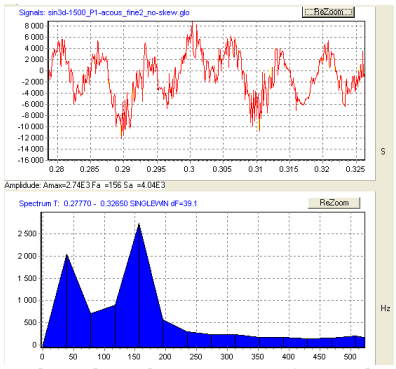

Fig. 22: Signal and spectrum for point P1; 3D computation

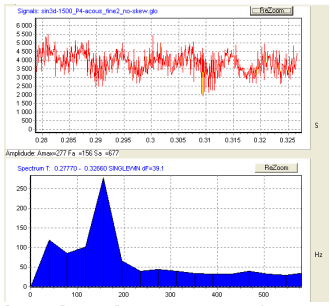

Fig. 23: Signal and spectrum for point P4; 3D computation

At the point P3 the numerical simulation does not give the spectrum obtained by measurements. The measured level of pressure pulsation and spectrum in P3 is essentially different from what is measured in points P1 and P4 and computed in P1, P2, P3 and P4. It can be assumed that there is some particularity in this measurement point, for example an orifice, which completely changes the pressure signal

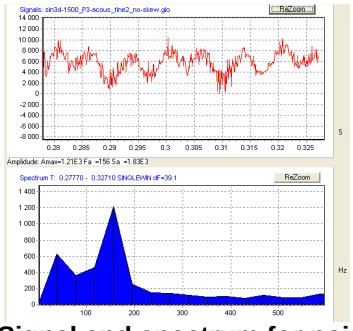

Fig. 24: Signal and spectrum for point P3; 3D computation

At the exit of pump the measured BPF component is rather small and the signal has a more stochastic character. Computation made under the grid of the first level shows the same behavior (Fig. 26).

Fig. 25: Spectrum plot (Bars) at point P5 (pump outlet)

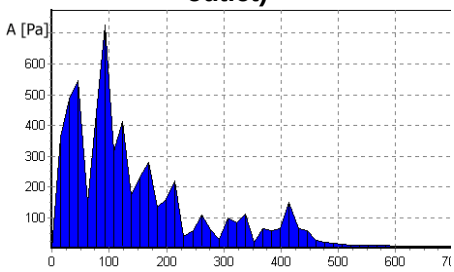

Fig. 26: Computed spectrum at point 5, outlet

3D CFD computation gives a continuous attenuation of the BPF amplitude along the volute length as it is shown in Fig. 27.

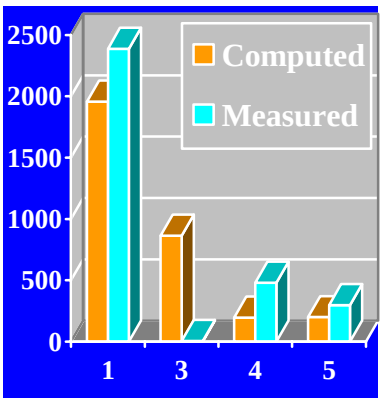

Fig. 27: Comparison of measurement with 3D computation (RMS-values)

INFLUENCE OF FLOW RATE AND IMPELLER DIAMETER

Computations are made for 3 operation modes with flow rates 30%, 100%, 120% of BEP flow rate and 2 diameters of impeller – 380 and 413 mm. (volute cutwater diameter D3 = 465mm) .Below one can see results for the point 1 in the volute.

IMPELLER 380 mm

Under the minimal flow rate (Fig. 28, Fig. 29) lower frequency components

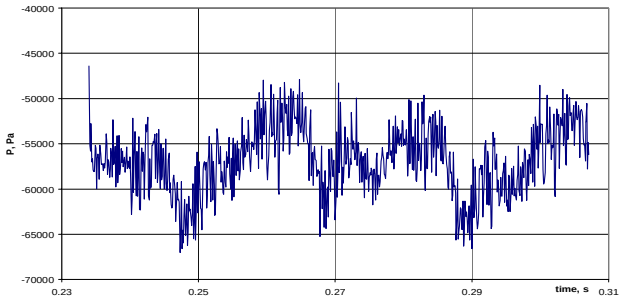

Fig. 28: Computed pressure signal at point 1 for Qmin

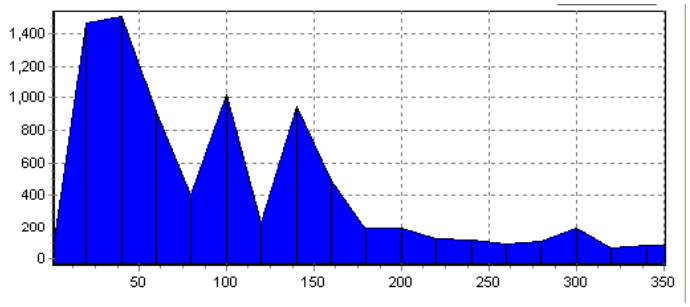

Fig. 29: Computed amplitude spectrum (Pa) for impeller 380 mm at the minimal flow rate Qmin

dominate in the signal. In the spectrum one can see amplitude level in Pa of the rotor frequency (25 Hz) and BPF (150 Hz).

For the nominal flow rate (Fig. 30, Fig. 31) BPF oscillations dominate in the spectrum and this agrees well with the measurement data. The computed pressure signal at point 1 has a distinct periodicity with the blade passing.

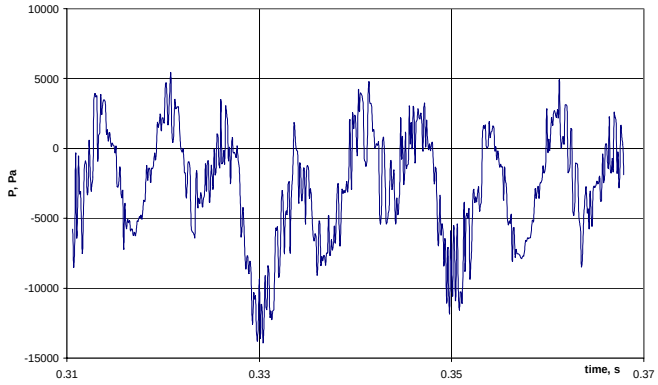

Fig. 30: Computed pressure signal at point 1 for Qnom

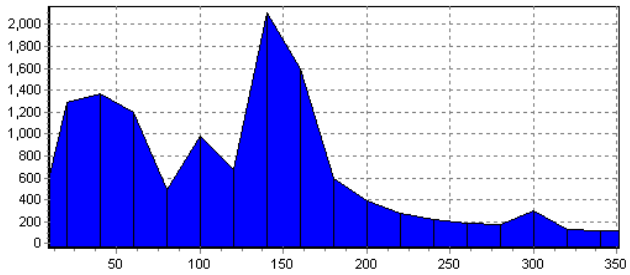

Fig. 31: Computed amplitude spectrum for impeller 380 mm at the nominal flow rate Qnom

At the maximal flow rate this BPF behavior of the pressure signal intensifies with increase of the main BPF tone by 50%.

IMPELLER 413 mm

With the increased diameter of impeller and at the minimal flow rate (Fig. 32, Fig. 33) the characteristic features of pressure pulsation strengthen.

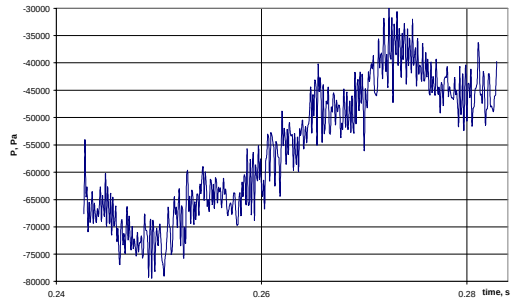

Fig. 32: Computed Pressure signal at point 1 for Qmin

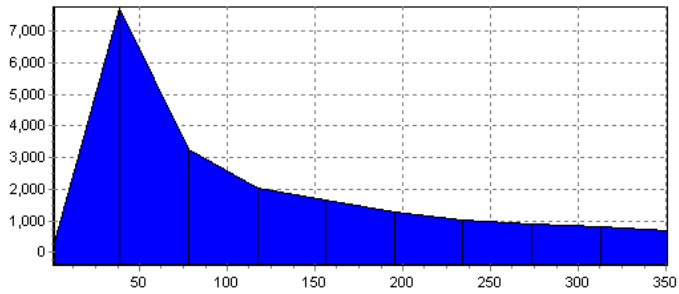

Fig. 33: Computed amplitude spectrum for impeller 413 mm at the minimal flow rate Qmin

For this operation mode the BPF component is negligible while oscillations has a strong periodicity with the rotor frequency.

At the nominal flow (Fig. 34, Fig. 35) rate BPF amplitude is very distinct and by 2 times higher than for the impeller 380 mm.

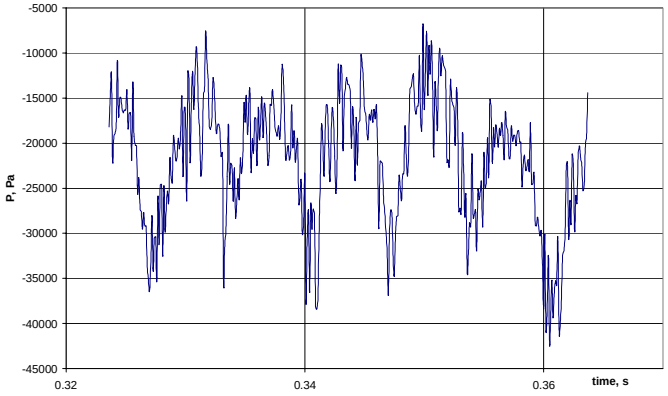

Fig. 34 Computed pressure signal at point 1 for Qnom

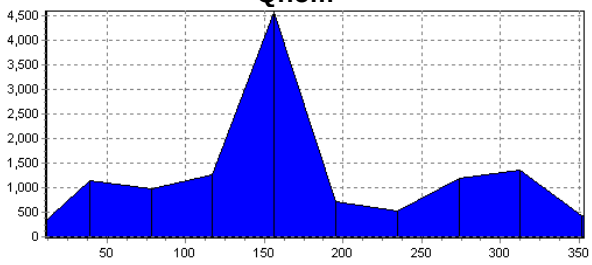

Fig. 35: Computed amplitude spectrum for impeller 413 mm at the nominal flow rate Qnom

For the maximal flow the blade passing periodicity is kept in the pressure pulsation signal but the shape of signal changes and it brings a slight reduction of the BPF main tone in the spectrum.

CONCLUSIONS

3D features of the flow of the diagonal pump cannot be treated by 2D method and agreement with the experimental data is reached only at the pump outlet for 2D prediction of pressure pulsation

Computational results reflect various features of the diagonal pump 3D unsteady flow, including inlet recirculation, secondary flow in the volute and BPF pressure pulsation

Reasonable agreement is obtained by 3D method for the head characteristic, using a limited number of grid cells.

3D unsteady computation shows an essential complex spatial behavior of the flow in the volute. Amplitude of pseudo-sound computed by 3D method agrees well with the experiment in the first region of volute closer to cutwater

Acoustical mode spectrum obtained on a rough grid (25000 cells) agrees with the experimental data; Distribution of BPF amplitude along the volute length is obtained using the new 3D CFD method.

Increasing of impeller diameter from 380 to 413 mm (reduction of the mean radial gap from 50 mm to 43 mm) gives amplification of the BPF tone in the volute by 2 times.

For the minimal flow rate (30% of BEP) in the pressure pulsation signal dominate lower frequency components – rotor frequency with its harmonics, while for the nominal and maximal flow rates the BPF main tone prevails over other components.

The pump inlet flow with geometry of 2 ribs can be an additional source of BPF type. Recirculation flow from the impeller (connected with rotating blades), can interact with inlet ribs in the same manner as the impeller outflow interacts with the bladed stator.

REFERENCES

[i] Timouchev S., Tourret J. Numerical Simulation of BPF Pressure Pulsation Field In Centrifugal Pumps. 19th International Pump Users Symposium, February 2002, Houston, Texas

[ii] D. Croba, J.L. Kueny. Unsteady flow computation in a centrifugal pump coupling of the impeller and the volute. Fan Noise. An International INCE Symposium. Senlis (France). Proceedings, 1992 pp.221 – 228

[iii] S. Chu, R. Dong, J. Katz. The effect of blade-tongue interactions on the flow structure, pressure fluctuations and noise within a centrifugal pump. Pump noise and vibrations. 1st International Symposium, Clamart (France), 1993 pp. 13 – 34

[iv] M.C. Thompson, K. Hourigan, A.N. Stokes. Prediction of the noise generation in a centrifugal fan by solution of the acoustic wave equation. Fan Noise. An International INCE Symposium. Senlis (France). Proceedings, 1992 pp. 197 – 204

[v] E. Manoha, S. Redonnet, C. Delahay, P. Segaut, I. Mary, S. Ben Khelil, P. Guillen Numerical prediction of the unsteady flow and radiated noise from a 3D lifting airfoil. Colloque: Bruit des Ventilateurs à Basse Vitesse, l'Ecole Centrale de Lyon, 8 et 9 novembre, 2001, Collection of papers

[vi] F. Perie, J. Buell Combined CFD/CAA method for centrifugal fan simulation. 29th international congress on noise control engineering, InterNoise 2000, Nice (France), Proceedings, 2000, v. 1, p.641

[vii] Timushev, S.F., Ovsyannikov, B.V. Pressure Fluctuation Numerical Simulation In A Centrifugal Pump Volute Casing. Journal de Physique IV, vol. 2. Second French Conference on Acoustics. Arcachon (France), 1992

[viii] J. Lighthill, Waves In Fluids Cambridge University Press 1978, p.60

ix J. Tourret et al. Hydraulic Noise Generation Studies in Centrifugal Turbomachine Through Visualization of the Non Stationary Pressure Field in the Volute and in the Impeller. ASME/ Reprinted From FED-Vol. 128, Experimental and Numerical Flow Visualization. Editors: B. Khalighi etc./Book No. 1991, pp.239 – 246.

[x] S. Timouchev, G. deBotton., A. Reznik Experimental and computational study of pressure pulsation in a centrifugal pump. 10th International Congress on Sound and Vibration, 7 10 July 2003, Stockholm, Sweden / Proceedings